ELSEVIER

Volume 181, Number 9, September 2008

JOURNAL OF SOLID STATE CHEMISTRY

www.elsevier.com/locate/jssc

CONTENTS

Abstracted/indexed in BioEngineering Abstracts, Chemical Abstracts, Coal Abstracts, Current Contents/Physics, Chemical, & Earth Sciences, Engineering Index, Research Alert, SCISEARCH, Science Abstracts, and Science Citation Index. Also covered in the abstract and citation database SCOPUS®. Full text available on ScienceDirect®.

Regular Articles

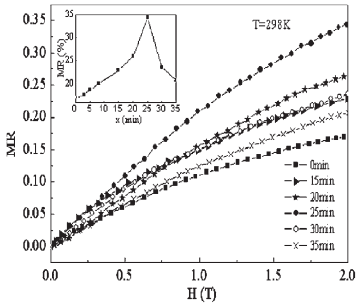

Magnetic field dependence of the MR for the composites at 298 K. The inset is the different silver-plating time dependence of the variation of MR at 2 T.

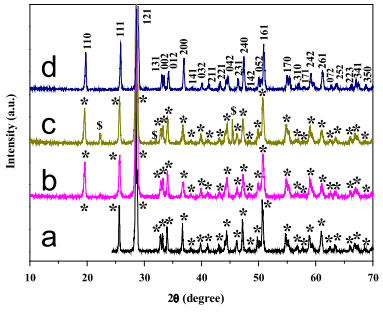

We described herein a facile solution-phase route to three nanocrystals of antimony oxychlorides and oxides ($Sb_4O_5Cl_2$, $Sb_8O_{11}Cl_2$, and Sb_2O_3). In particular, the solvent composition controlled the selective preparation of cubic Sb_2O_3 (senarmontite) and orthorhombic Sb_2O_3 (valentinite).

Regular Articles—Continued

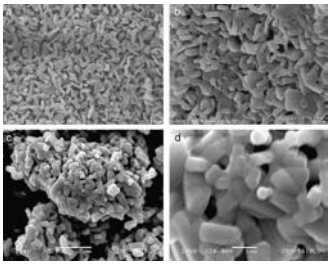

The $K_6Nb_{10.8}O_{30}$ powders with TB-type structure were synthesized by a wet chemical method at lower temperature. The particle size of the as-prepared powders is much smaller than that of the sample by obtained solid-state method and its photocatalytic activity is much higher than that of the latter and slightly higher than that of P25-TiO_2.

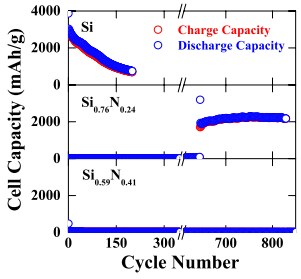

The $Si_{0.76}N_{0.24}$ thin films showed negligible initial capacity, but an abrupt capacity increase to ~2300 mA h/g after ~650 cycles, followed by excellent cycle-life performance. This abnormal electrochemical behavior was demonstrated to be correlated with the formation of Li_3N and Si_3N_4.

Precipitation of $ALn(CO_3)_2, xH_2O$ and $Dy_2(CO_3)_3, xH_2O$ compounds from aqueous solutions for $A^+ = Li^+$, Na^+, K^+, Cs^+, NH_4^+ and $Ln^{3+} = La^{3+}$, Nd^{3+}, Eu^{3+}, Dy^{3+}
Violaine Philippini, Thomas Vercouter, Annie Chaussé and Pierre Vitorge
Page 2143

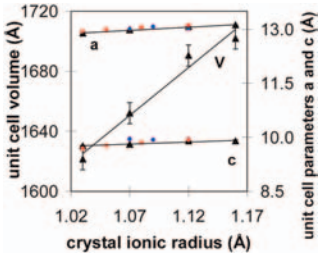

Linear relationships between the ionic radii of the lanthanides and the unit cell parameters of the corresponding $NaLn(CO_3)_2, xH_2O$ compounds, extracted from three different studies (our experimental data (black) are compared with those of Mochizuki et al. (red) and Runde et al. (blue)).

Synthesis and study of the crystallographic and magnetic structure of $DyFeMnO_5$: A new ferrimagnetic oxide
M.J. Martínez-Lope, M. Retuerto, J.A. Alonso and V. Pomjakushin
Page 2155

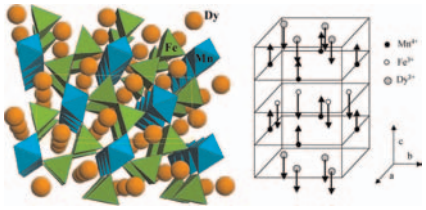

$DyFeMnO_5$ is orthorhombic (*Pbam*) as the parent $DyMn_2O_5$ oxide. The crystal structure contains infinite chains of edge-sharing $Mn^{4+}O_6$ octahedra, interconnected by dimer units of $Fe^{3+}O_5$ square pyramids. It is ferrimagnetic below $T_C \approx 178$ K; a NPD study indicated an antiferromagnetic coupling of the Mn^{4+} and Fe^{3+} spins, with Dy^{3+} magnetic moments parallel to those of Fe.

Photoluminescence of Eu^{3+}-doped triple phosphate $Ca_8MgR(PO_4)_7$ (R = La, Gd, Y)
Yanlin Huang, Wanxue Zhao, Yonggang Cao, Kiwan Jang, Ho Sueb Lee, Eunjin Cho and Soung-Soo Yi
Page 2161

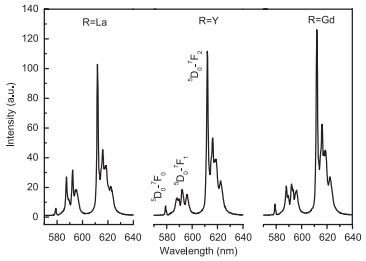

The RT luminescence spectra of $Ca_8MgR(PO_4)_7$ (R = La, Gd, Y) under 254 nm excitation using lamp source with the same conditions. The red emission lines at 612 nm originating from the electric dipole transition $^5D_0$–$^7F_2$ is the dominant luminescence in the spectrum. It is found that the emission intensity of Eu^{3+} ions in $Ca_8MgR(PO_4)_7$ (R = La, Gd, Y) decreases in the sequence of R = Gd > Y > La.

A sodium gadolinium phosphate with two different types of tunnel structure: Synthesis, crystal structure, and optical properties of $Na_3GdP_2O_8$
M. Fang, W.-D. Cheng, H. Zhang, D. Zhao, W.-L. Zhang and S.-L. Yang
Page 2165

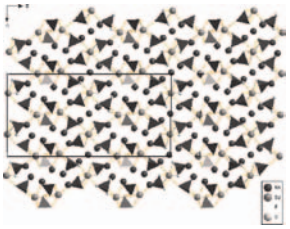

Projection of the structure of $Na_3GdP_2O_8$ with a unit cell edge along the *b*-axis. The Na–O bonds are omitted for clarity.

Structure and morphology controllable synthesis of Ag/carbon hybrid with ionic liquid as soft-template and their catalytic properties
Shu Ying Wu, Yun Sheng Ding, Xiao Min Zhang, Hai Ou Tang, Long Chen and Bo Xuan Li
Page 2171

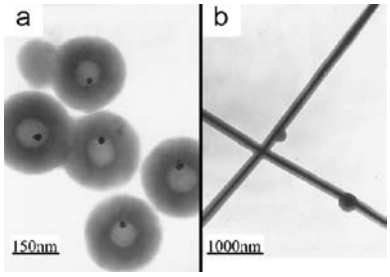

Monodisperse carbon hollow nanospheres encapsulating Ag nanoparticles and Ag/carbon nanocables were selectively prepared with ionic liquids as the soft-template. The controllable synthesis of Ag/C nano-hybrids was realized by varying the concentration of ionic liquids, reaction temperature, reaction time and the mole ratio of silver nitrate to glucose. The catalysis of Ag/C nano-hybrid in the oxidation of 1-butanol by H_2O_2 was also investigated.

Syntheses, crystal structures and properties of two 1-D cadmium(II) coordination polymers based on 1,1′-(1,3-propanediyl)bis-1H-benzimidazole
Huaixia Yang, Xiangru Meng, Yun Liu, Hongwei Hou, Yaoting Fan and Xiaoqing Shen
Page 2178

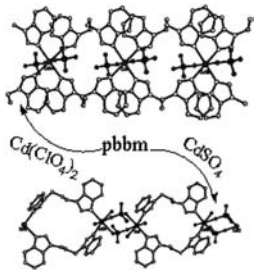

Two new Cd(II)-containing complexes have been synthesized and characterized by single-crystal X-ray diffraction. The antimicrobial activity and the non-isothermal kinetics of the thermal decomposition of the polymers were also investigated.

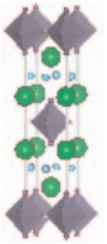

The K_2NiF_4-type phase Ba_2SnO_4 has been fluorinated at 240 °C using ZnF_2 to give a new oxide fluoride of composition $Ba_2SnO_{2.5}F_3 \cdot xH_2O$ ($x \approx 0.5$). A model in which fluorine occupies both interstitial and apical substitutional sites in the structure of the precursor oxide is supported by spectroscopic and diffraction information, combined with atomistic computer modelling studies.

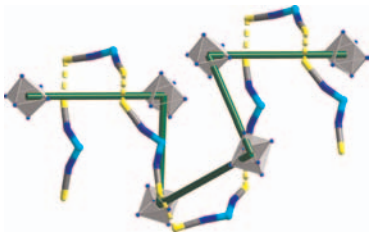

Side projection in **2** showing the crankshaft caused by S···S interactions in $[Co(NCS)_4]^{2-}$ in-between $[Ru^{II}(phen)_3]^{2+}$ helices. Only isothiocyanates arms of $[Co(NCS)_4]^{2-}$ that are part of S···S interactions are shown and $[Ru^{II}(phen)_3]^{2+}$ are presented as polyhedra.

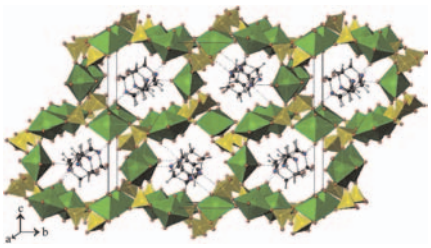

Packing diagram of the three-dimensional channels and occluded $DABCOH_2^{2+}$ and water molecules found in $[C_6H_{14}N_2][(UO_2)_4(HPO_4)_2(PO_4)_2(H_2O)] \cdot H_2O$.

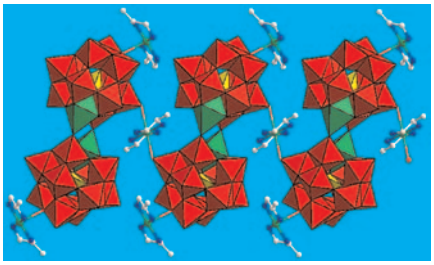

A family of inorganic–organic composite polyoxotugstates have been harvested by combination of in-situ generated monocopper^{II}-substituted Keggin polyoxoanions and copper^{II}–organoamine complexes based on di-/tri-/hexa-vacant polyoxoanion precursors, $CuCl_2 \cdot 2H_2O$ and organoamines under hydrothermal conditions and structurally characterized by the elemental analysis, IR spectroscopy, TGA and single-crystal X-ray crystallography.

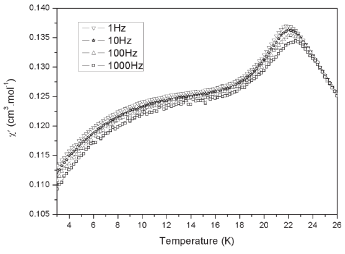

The $n = 1$ Ruddlesden–Popper system $Pr_{3-x}Sr_{1+x}CrNiO_8$ ($0.0 < x \leqslant 1.0$) has been characterized by diffraction methods and magnetometry. There is no evidence of Cr/Ni cation ordering in any composition. The atomic magnetic moments adopt a spin-glass-like state below a transition temperature that decreases from 52 K ($x = 0.1$) to 13 K ($x = 1.0$).

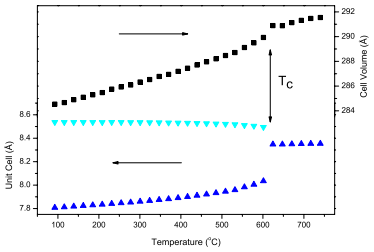

The first-order tetragonal–cubic phase transition in $CuCr_2O_4$ is accompanied by a noticeably reduction in cell volume associated with the loss of orbital ordering present in the low-temperature Jahn–Teller distorted tetragonal structure.

Continued

Synthesis of nanospherical Fe_3BO_6 anode material for lithium-ion battery by the rheological phase reaction method
Xixi Shi, Caixian Chang, Jiangfeng Xiang, Yong Xiao, Liangjie Yuan and Jutang Sun
Page 2231

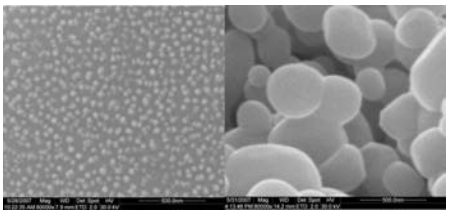

Nanospherical Fe_3BO_6 anode material for lithium-ion battery has been synthesized by the rheological phase reaction method. The electrochemical properties of these Fe_3BO_6 nanospheres show that sample synthesized at 800 °C delivers a high reversible capacity above 500 mAh g^{-1}, and sample synthesized at 900 °C possesses relatively good cycleability with a capacity retaining of 376 mAh g^{-1} after 10 cycles.

Hydrothermal assembly and luminescence property of lanthanide-containing Anderson polyoxometalates
Ying Liu, Shu-Xia Liu, Rui-Ge Cao, Hong-Mei Ji, Shi-Wei Zhang and Yuan-Hang Ren
Page 2237

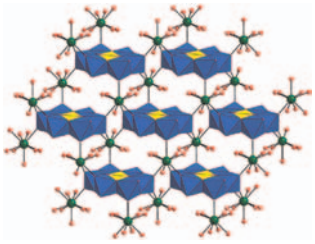

Two compounds based on Anderson-type polyoxoanion building blocks and rare-earth ions have been synthesized under hydrothermal conditions. Compound **1** exhibits a 2D layer architecture constructed from $[TeMo_6O_{24}]^{6-}$ anions and rare-earth ions Ln^{3+}. Compound **2** displays a 1D chain structure and possesses the intense luminescence property.

Phase formation, structural and microstructural characterization of novel oxynitride–perovskites synthesized by thermal ammonolysis of (Ca,Ba)MoO_4 and (Ca,Ba)MoO_3
D. Logvinovich, M.H. Aguirre, J. Hejtmanek, R. Aguiar, S.G. Ebbinghaus, A. Reller and A. Weidenkaff
Page 2243

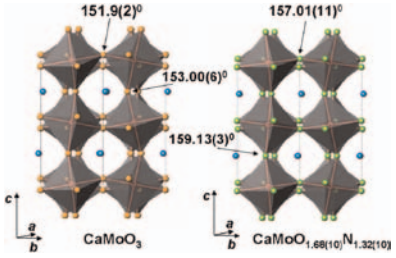

Reactions of $AMoO_4$ and $AMoO_3$ ($A = Ca^{2+}$, Ba^{2+}) oxides with ammonia have been studied at $T = 873$–1123 K. Orthorhombic $CaMoO_{1.7(1)}N_{1.3(1)}$ (*Pbnm*) and cubic $BaMo(O,N)_3$ ($Pm\bar{3}m$) were prepared by thermal ammonolysis of the corresponding $CaMoO_3$ and $BaMoO_3$ precursors at $T = 898$ and 998 K, respectively.

The role of the coordination defect: A new structural description of four fluorite-related sesquioxide minerals, bixbyite (Mn_2O_3), braunite (Mn_7SiO_{12}), braunite II ($CaMn_{14}SiO_{24}$), parwelite ($Mn_{10}Sb_2As_2Si_2O_{24}$), and their structural relationships
D.J.M. Bevan and R.L. Martin
Page 2250

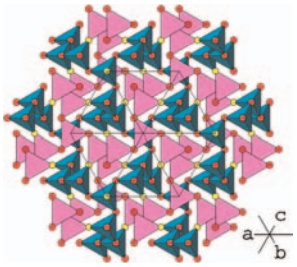

The anion-deficient, fluorite-related structures of the manganese-based minerals bixbyite (Mn_2O_3), braunite (Mn_7SiO_{12}), braunite II ($CaMn_{14}SiO_{24}$) and parwelite ($Mn_{10}Sb_2As_2Si_2O_{24}$), are reinterpreted in terms of the Coordination Defect (CD) theory to gain new insights into their structural interrelationships. CDs are extended, defects centred by an anion vacancy and including its immediate atomic environment of 4 tetrahedrally coordinated metals and 6 octahedrally coordinated O atoms: it is represented as $\square M_4O_6$, where the symbol $\square$ is the anion vacancy. The arrangement of $\square M_4$ tetrahedra in bixbyite is shown in the [111] projection.

Polymorphism in PbBiO$X$$O_4$ compounds (X = V, P, As). Part I: Crystal structures of α- and β-PbBiOVO_4
Olfa Labidi, Pascal Roussel, Florence Porcher, Michel Drache, Rose-Noëlle Vannier and Jean-Pierre Wignacourt
Page 2260

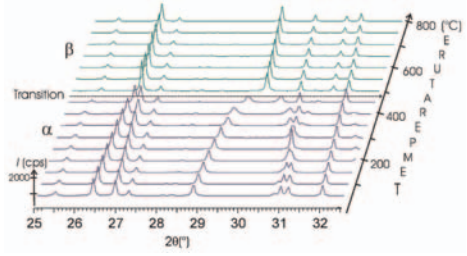

PbBiOVO_4 polymorphism.

Polymorphism in PbBiO$X$$O_4$ compounds (X = V, P, As): Part II—PbBiOPO_4 and PbBiOAsO_4 structures and characterization of related solid solutions
Olfa Labidi, Pascal Roussel, Michel Drache, Rose-Noëlle Vannier and Jean-Pierre Wignacourt
Page 2268

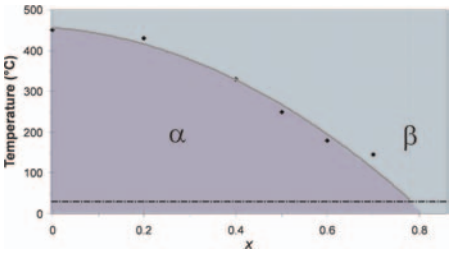

$\alpha \rightarrow \beta$ PbBiO$V_{1-x}As_xO_4$ composition dependence.

Fabrication and characterization of hexagonal boron nitride powder by spray drying and calcining–nitriding technology
Xiaoliang Shi, Sheng Wang, Hua Yang, Xinglong Duan and Xuebin Dong
Page 2274

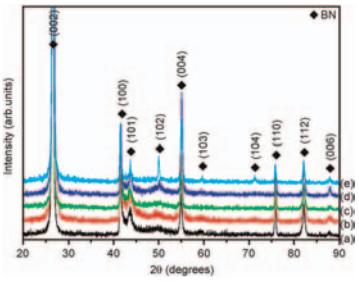

hBN powder was fabricated prepared by spray drying and calcining–nitriding technology. The results indicated that spray drying and calcining–nitriding technology assisted with high-energy ball-milling process following calcined process was a hopeful way to manufacture hBN powder with high crystallinity in industrial scale.

Synthesis and properties of transparent luminescent nanocomposites with surface functionalized semiconductor nanocrystals
Junfang Gao, Yuqin Fu, Xiaodan Lü, Yaying Du, Changli Lü and Zhongmin Su
Page 2279

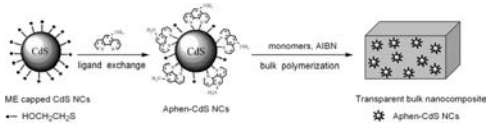

Transparent luminescent nanocomposites with Aphen functionalized CdS nanocrystals were synthesized by ligand exchange and in-situ bulk polymerization. The functionalized nanocrystals and their polymer nanocomposites possessed strong luminescent emission and can be potentially used to fabricate multifunctional devices with novel photoelectric properties.

Aluminium substitution in iron(II–III)-layered double hydroxides: Formation and cationic order
Christian Ruby, Mustapha Abdelmoula, Rabha Aissa, Ghouti Medjahdi, Michela Brunelli and Michel François
Page 2285

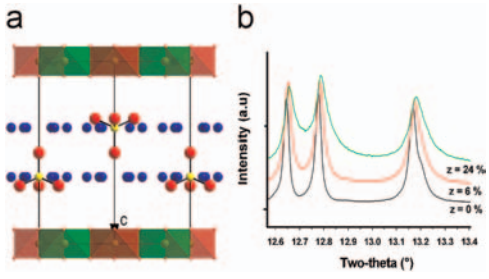

(a) Crystallographical structure of sulphated green rust: SO_4^{2-} point to the Fe^{3+} cations (red) that form an ordered array with the Fe^{2+} cations (green). (b) Width and asymmetry of the synchrotron XRD peaks increase rapidly when some Al^{3+} species substitute the Fe^{3+} cations; z is molar ratio Al^{3+}/Fe^{3+}.

Neutron powder diffraction study of the magnetic and crystal structures of $SrFe_2(PO_4)_2$
Alexei A. Belik, Qingzhen Huang, Eiji Takayama-Muromachi and Jeffrey W. Lynn
Page 2292

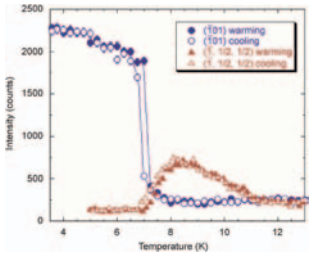

Temperature dependence of the intensities of representative magnetic reflections (-101) and $(-1,\frac{1}{2},\frac{1}{2})$ during cooling and heating in $SrFe_2(PO_4)_2$.

Characterization of CoMCM-41 mesoporous molecular sieves obtained by the microwave irradiation method
Tingshun Jiang, Wei Shen, Qian Zhao, Mei Li, Jinyu Chu and Hengbo Yin
Page 2298

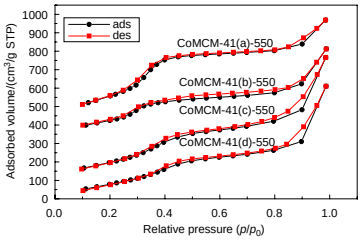

CoMCM-41 mesoporous molecular sieves with different amounts of cobalt were synthesized via the microwave irradiation method. The samples were characterized by X-ray diffraction (XRD), Fourier transform infrared (FT-IR), temperature programmed reduction (TPR), transmission electron microscopy (TEM) and N_2 adsorption–desorption technique, and thermal and hydrothermal stabilities of synthesized CoMCM-41 samples were also investigated. The results show that these synthesized materials have typical MCM-41 structure and highly thermal and hydrothermal stabilities.

Structure and phase composition of nanocrystalline $Ce_{1-x}Lu_xO_{2-y}$
Małgorzata A. Małecka, Leszek Kępiński and Mirosław Mączka
Page 2306

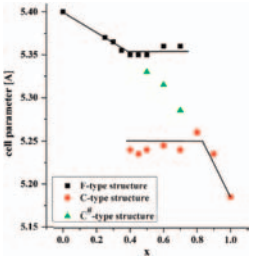

Phase separation in nanocrystalline $Ce_{1-x}Lu_xO_{2-y}$ mixed oxide heated in air at 1100 °C.

Continued

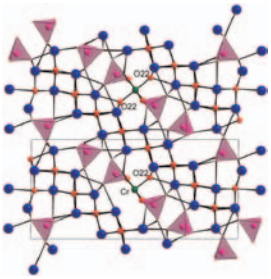

View of $Bi_{6.24}Cr_{0.09}P_2O_{14.4}$ perpendicular to [010].

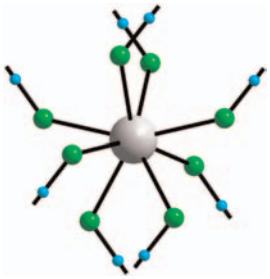

Three new compounds $Ca(HF_2)_2$, $Ba_4F_4(HF_2)(PF_6)_3$ and $Pb_2F_2(HF_2)(PF_6)$ were obtained in the system metal(II) fluoride and anhydrous HF acidified with excessive PF_5 and characterized by X-ray single crystal diffraction method and partly by Raman spectroscopy. $Ca(HF_2)_2$ represents the second known compound with homoleptic HF_2^- environment of the central atom.

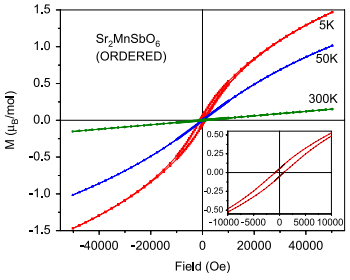

The M vs. H plots for the ordered Sr_2MnSbO_6. The magnetization data at 5 K shows hysteresis loop (inset) with a Brillouin-like curvature indicating significant ferromagnetic correlations in the system.

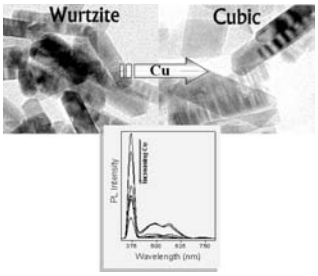

ZnS nanorods doped with 0–15 mol% of Cu has been prepared by simple solvothermal route. Interestingly, phase transformation of the doped ZnS nanorods from wurtzite to cubic was observed with gradual increase in the Cu concentration. Doped ZnS nanorods showed luminescence over a wide range from UV to near IR, which is also a rare observation.

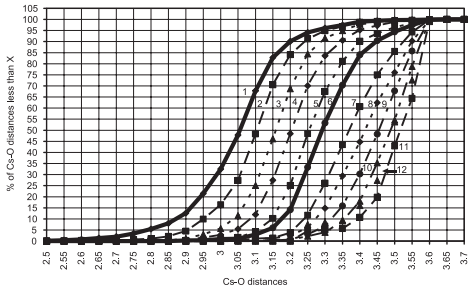

A survey of more than 1000 of oxygen polyhedrons around caesium ions shows bond lengths ranging from 2.46 to 3.60 Å with 32% of the shortest bonds in the polyhedrons less than 3.00 Å. Coordination numbers from 1 to 12 are observed, in which the average bond lengths increase from 2.714 to 3.323 Å with the coordination, and with a preference for 8, 9 and 10-fold surrounding.

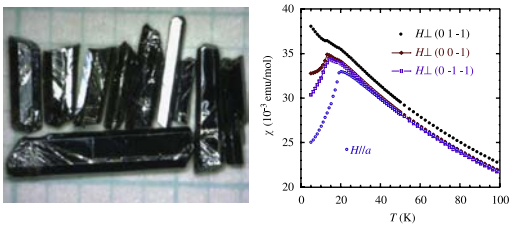

$FeVO_4$ (**I**) single crystals are grown by the flux method using V_2O_5 as the self-flux. Magnetic properties are investigated by means of magnetic susceptibility, magnetization, and heat capacity measurements, showing two magnetic phase transitions at ~13 and ~20 K.

Reactivity of metal oxides: Thermal and photochemical dissolution of *M*O and MFe_2O_4 (*M* = Ni, Co, Zn)
Luis A. García Rodenas, Miguel A. Blesa and Pedro J. Morando
Page 2350

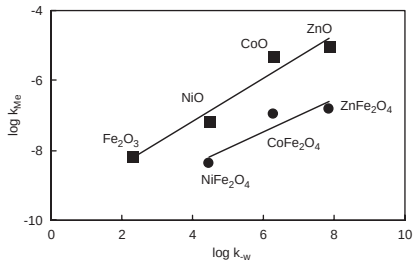

Linear relationships between k_{Me} and k_{-w} are observed. In ferrites, Fe(III) arrests more the reactivity of the more labile ions, thus producing a lower slope.

Direct synthesis of silver/polymer/carbon nanocables via a simple hydrothermal route
Mingshang Jin, Qin Kuang, Zhiyuan Jiang, Tao Xu, Zhaoxiong Xie and Lansun Zheng
Page 2359

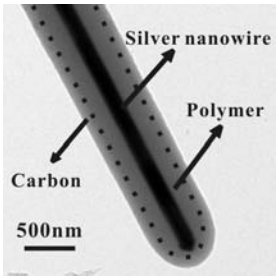

High-yield silver/polymer/carbon coaxial nanocables were synthesized via a one-step simple hydrothermal route by using silver chloride and glucose as precursors. Our experiments indicate that such novel nanostructures formed through the growth mechanism that the silver nanowires grow first, and then glycosidation of glucose occurs on the silver nanowire surfaces, and finally the partial carbonization occurs on the outmost surface of the polymer layer.

Temperature dependence of the cation distribution in $ZnFe_2O_4$ measured with high temperature neutron diffraction
F. Bræstrup, B.C. Hauback and K.K. Hansen
Page 2364

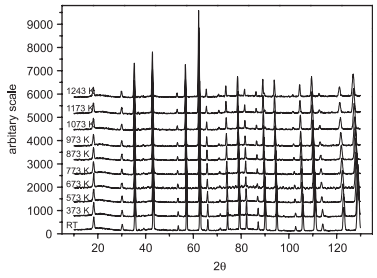

High temperature in situ neutron powder diffraction, dilatometry and resistivity measurements was performed on the spinel-type oxide $ZnFe_2O_4$.

Solvothermal syntheses, and characterization of $[Ln(en)_4(SbSe_4)]$ (*Ln* = Ce, Pr) and $[Ln(en)_4]SbSe_4 \cdot 0.5en$ (*Ln* = Eu, Gd, Er, Tm, Yb): The effect of lanthanide contraction on the crystal structures of lanthanide selenidoantimonates(V)
Dingxian Jia, Aimei Zhu, Qinyan Jin, Yong Zhang and Wenqing Jiang
Page 2370

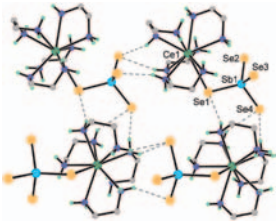

Two types of lanthanide selenidoantimonates $[Ln(en)_4(SbSe_4)]$ (*Ln* = Ce, Pr) and $[Ln(en)_4]SbSe_4 \cdot 0.5en$ (*Ln* = Eu, Gd, Er, Tm, Yb; en = ethylenediamine) have been synthesized under the mild solvothermal conditions, and a systematic investigation of the crystal structures reveals that two types of structural features of these lanthanide selenidoantimonates are related with lanthanides contraction across the lanthanide series.

Hydrothermal syntheses, crystal structures and properties of three coordination frameworks based on a new semirigid ligand and benzenedicarboxylate
Yao-Mei Fu, Ya-Hui Zhao, Ya-Qian Lan, Kui-Zhan Shao, Yong-Qing Qiu, Xiang-Rong Hao and Zhong-Min Su
Page 2378

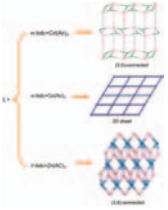

Three unprecedented complexes have been constructed from a new semirigid ligand 1,1′-bis(pyridin-3-ylmethyl)-2,2′-biimidazole (**L**) combined with benzenedicarboxylate isomers and different metal ions under hydrothermal conditions, which exhibit novel topologies. Luminescent properties of **L** ligand, compounds **1** and **3** are also determined.

Isomorphous substitution of europium for strontium in the structure of synthetic hydroxovanadate
E.I. Get'man, N.V. Yablochkova, S.N. Loboda, V.V. Prisedsky, V.P. Antonovich and N.A. Chivireva
Page 2386

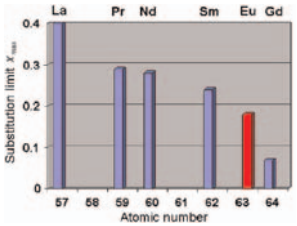

The results of this paper contribute to a general picture of substitution effects of the rare-earth (RE) elements in the apatite structure. The dependence of the substitution limit x_{max} in $Sr_{10-x}RE_x(VO_4)_6(OH)_{2-x}O_x$ on the atomic number of the RE element is shown here with the present data marked with red color.

Continued

Phase relations in the $K_2W_2O_7$–K_2WO_4–KPO_3–Bi_2O_3 system and structure of $K_{6.5}Bi_{2.5}W_4P_6O_{34}$
K.V. Terebilenko, I.V. Zatovsky, V.N. Baumer, I.V. Ogorodnyk, N.S. Slobodyanik and O.V. Shishkin
Page 2393

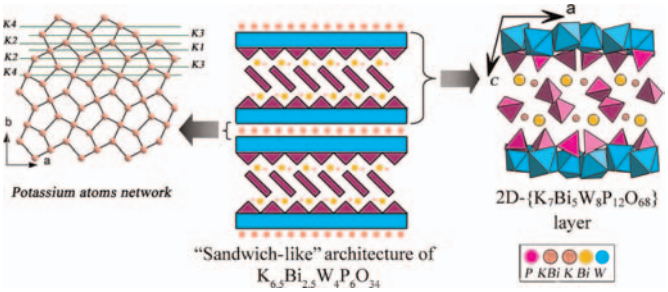

Sandwich-like architecture of $K_{6.5}Bi_{2.5}W_4P_6O_{34}$ prepared during high-temperature investigation of $K_2W_2O_7$–K_2WO_4–KPO_3 system. It is organized from $\{K_7Bi_5W_8P_{12}O_{68}\}_\infty$ layers and potassium atom sheets.

One-step synthesis of hydrothermally stable mesoporous aluminosilicates with strong acidity
Dongjiang Yang, Yao Xu, Dong Wu and Yuhan Sun
Page 2401

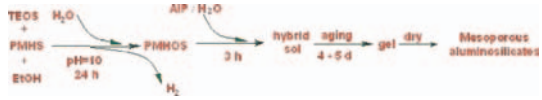

Based on the nonsurfactant method, a facile one-step synthesis route has been developed to prepare methyl-modified mesoporous aluminosilicates that possessed hydrothermal stability and strong acidity.

Two unprecedented 1D coordination polymer chains based on tetranuclear copper(II) building blocks
Gaijuan Li, Yan Xing, Shuyan Song, Ning Xu, Xianchun Liu and Zhongmin Su
Page 2406

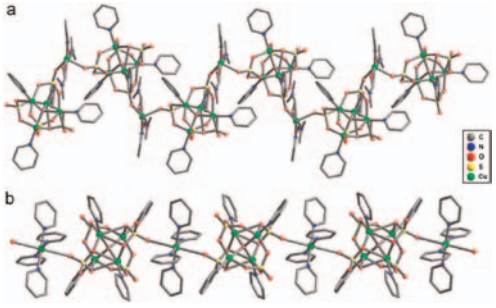

Two unprecedented Cu(II) coordination polymers have been prepared by using solvothermal method; they consist of tetrahedral tetranuclear clusters that are bridged by unique Cu(II) atom through the sulfate oxygen to form the infinite one-dimensional polymer chains (a) for complex **1** and (b) for complex **2**.

Computerized crystal-chemical classification of silicates and related materials with CRYSTANA and formula notation for classified structures
Hans-Joachim Klein and Friedrich Liebau
Page 2412

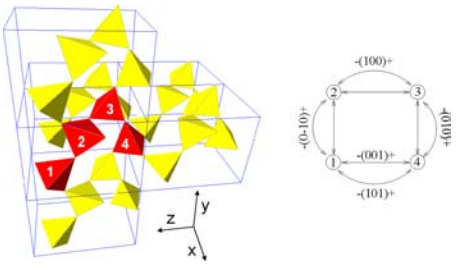

The computer program CRYSTANA is described which implements a method for the crystal-chemical classification of silicates and related materials. The implementation is based upon a graph-theoretical formalization of the classification method. An extended notation of crystal-chemical formulas is introduced. The formulas can be derived from the output of the program.

Role of crystallite size on the photoluminescence properties of $SrIn_2O_4$:Eu^{3+} phosphor synthesized by different methods
N. Lakshminarasimhan and U.V. Varadaraju
Page 2418

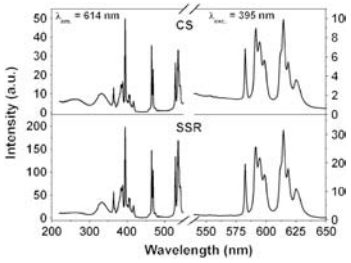

Comparison of PL excitation and emission of Eu^{3+} in $SrIn_2O_4$ synthesized by solid state reaction (SSR) and combustion synthesis (CS) methods revealing a decrease in intensity for CS method.

Preparation and characterization of (SBA-15)–La_2O_3 host–guest composite materials
Hui Yu and Qing-Zhou Zhai
Page 2424

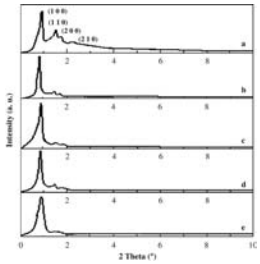

Lanthanum oxide was successfully incorporated into SBA-15 mesoporous molecular sieve via the microwave-assisted synthesis method (MASM) for the first time. The results showed that the preparation of (SBA-15)–La_2O_3 host–guest composite materials by MASM has the advantages of simpler operation, higher efficiency and more plentiful lanthanum oxide can be incorporated into SBA-15 compared with other methods.

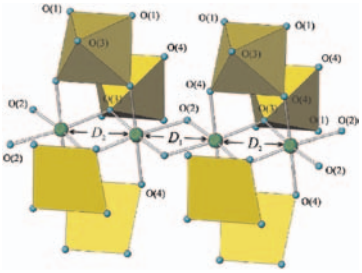

Alternating Cr–Cr separations in the chain of edge-sharing CrO_6 octahedra and the constraining effect of the GeO_5 square pyramids in the structures of $RCrGeO_5$.

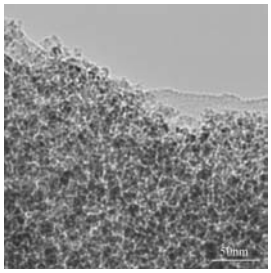

We report the preparation of SiO_2 glass by consolidating a highly dispersed silicic acid powder with the Spark Plasma Sintering (SPS) technique. The glass was characterized by ellipsometry, transmission electron microscopy (TEM), infrared reflectance and transmittance spectroscopy, as well as by Raman-, UV–Vis–NIR- and solid-state nuclear magnetic resonance (NMR) spectroscopy.

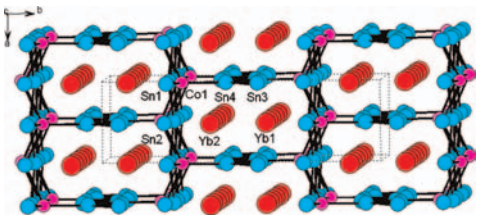

Yb_3CoSn_6 and $Yb_4Mn_2Sn_5$ have been prepared and structurally characterized. Yb_3CoSn_6 features a 3D open-framework composed of novel $[CoSn_3]$ layers interconnected by the zigzag Sn chains whereas the anionic substructure of $Yb_4Mn_2Sn_5$ is composed of parallel $[Mn_2Sn_2]$ ladders interconnected by the unusual one-dimensional (1D) chains formed by linear $[Sn_3]$ trimers.

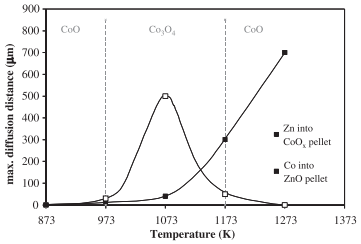

Maximum diffusion distance for the ZnO–CoO_x couple as a function of temperature. Dashed gray lines represent the temperature values at which the transformations between CoO and Co_3O_4 compounds take place.

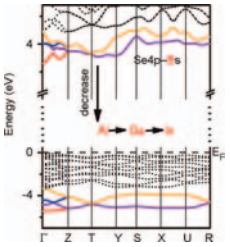

The electronic structures and optical properties of wurtzite type $LiBSe_2$ (B = Al, Ga, In) have been studied by the DFT calculations. And the correlation of the electronegative of B element and the band gap decrease-trend are discussed. The comparison between different calculation methods and the experimental results is presented.

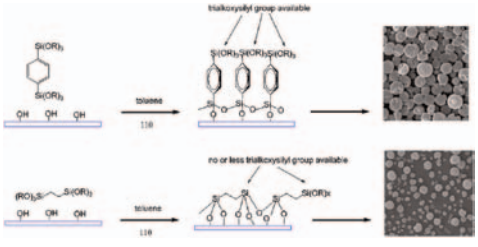

1, 4-diisocyanatobutane (DICB) was used as the covalent molecular linker in this study to prepare the uniformly oriented zeolite L monolayer with a relatively high coverage degree and close packing degree. This could be ascribed to substantial amounts of DICB self-assemble and standing on the substrate surface instead of folding up into a U-shape. This point has been further verified by the quality of oriented zoelite L monolayers obtained from the procedure involving DICB, 1, 4-bis (triethoxysilyl) benzene (BTSEB) and 1,2-bis(trimethoxysilyl)ethane (BTMSE) as covalent molecular linkers.

Continued

Hyperfine interactions and lattice dynamics of $Sn_{21}O_6Cl_{16}(OH)_{14}$
M.T. Sougrati, S. Jouen, B. Hannoyer and B. Lefez
Page 2473

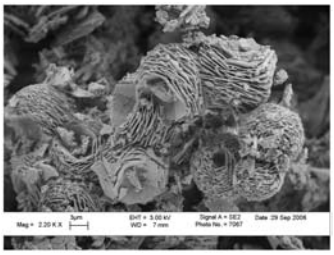

In this study, the tin(II) oxy-hydroxychloride $Sn_{21}O_6Cl_{16}(OH)_{14}$ has been synthesised. The Mössbauer parameters determined at various temperatures are reported and discussed for the first time. At room temperature, the isomer shift and the quadrupole splitting of $Sn_{21}O_6Cl_{16}(OH)_{14}$ are, respectively, $\delta = 3.22\,mm\,s^{-1}$ and $\Delta = 1.71\,mm\,s^{-1}$ and the recoil-free fraction at 300 K is $f_{300} = 0.09 \pm 0.02$.

Structure, bonding and physical properties of tetragonal and orthorhombic SiS_2 from (hybrid) DFT calculations
Martijn A. Zwijnenburg, Robert G. Bell and Furio Corà
Page 2480

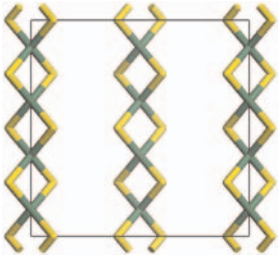

Periodic DFT calculations were employed to study the (physical) properties of tetragonal and orthorhombic SiS_2. The results obtained were compared with those for SiS_2 better studied oxide analog silica and demonstrate large changes in the materials' energy landscape, nature of bonding, flexibility and band gap, upon substitution of sulphur for oxygen.

Lanthanide complexes of the monovacant Dawson polyoxotungstate $[\alpha_2\text{-}As_2W_{17}O_{61}]^{10-}$ with 1D chain: Synthesis, structures, and photoluminescence properties
Xin-Yu Zhao, Shu-Xia Liu, Yuan-Hang Ren, Jian-Fang Cao, Rui-Ge Cao and Kui-Zhan Shao
Page 2488

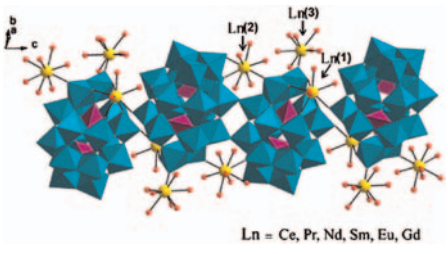

Six new lanthanide complexes based on monovacant Dawson-type tungstoarsenates have been synthesized. These complexes are one-dimensional chain-like structures constructed by lanthanide cations and $[\alpha_2\text{-}As_2W_{17}O_{61}]^{10-}$ anions. There are three kinds of coordination environment for lanthanide cations. Photoluminescence measurement reveals that **4** and **5** exhibit orange and red fluorescent emission at room temperature, respectively.

Type A–B carbonate chlorapatite synthesized at high pressure
Michael E. Fleet and Xi Liu
Page 2494

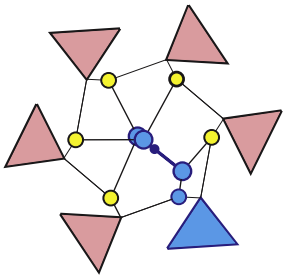

Defect cluster (blue) of A carbonate ion in apatite channel, Na^+ cation, and B carbonate ion replacing phosphate group, in carbonate chlorapatite synthesized at high pressure.

Structure and oxide anion conductivity in $Ln_2(TO_4)O$ (Ln = La, Nd; T = Ge, Si)
Laura León-Reina, José M. Porras-Vázquez, Enrique R. Losilla, Laureano Moreno-Real and Miguel A.G. Aranda
Page 2501

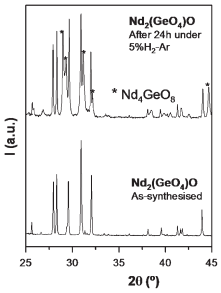

$Ln_2(TO_4)O$ oxy-silicates and oxy-germanates show ionic conductivities $\sim 10^{-4}\,S\,cm^{-1}$ at 1173 K with p-type electronic contribution under oxidising conditions. Furthermore, the studied materials are not stable under strongly reducing conditions as shown in the attached figure.

Anchored thiol smectite clay—kinetic and thermodynamic studies of divalent copper and cobalt adsorption
Denis Lima Guerra and Claudio Airoldi
Page 2507

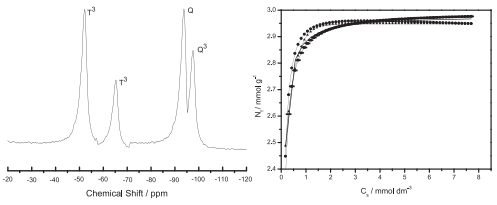

A natural smectite clay sample from Serra de Maicuru, Pará State, Brazil, had aluminum and zirconium polyoxycations inserted within the interlayer space. The precursor and pillarized smectites were organofunctionalized with the silyating agent 3-mercaptopropyltrimethoxysilane. These chemically immobilized clay samples adsorb divalent copper and cobalt cations from aqueous solutions of pH 5.0 at 298 ± 1 K. The Langmuir, Redlich–Peterson and Toth adsorption isotherm models have been applied to fit the experimental data with a nonlinear approach.

Hierarchical chlorine-doped rutile TiO_2 spherical clusters of nanorods: Large-scale synthesis and high photocatalytic activity

Hua Xu, Zhi Zheng, Lizhi Zhang, Hailu Zhang and Feng Deng

Page 2516

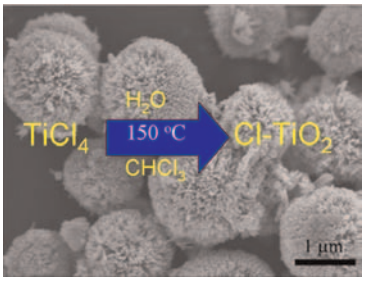

Hierarchical chlorine-doped rutile TiO_2 spherical clusters of nanorods photocatalyst were synthesized on a large scale via a soft interface approach. This catalyst showed much higher photocatalytic activity than the famous commercial titania (Degussa P25) under visible light ($\lambda > 420$ nm).

Crystal structures and chemistry of double perovskites $Ba_2M(II)M'(VI)O_6$ (M = Ca, Sr, M' = Te, W, U)

W.T. Fu, Y.S. Au, S. Akerboom and D.J.W. IJdo

Page 2523

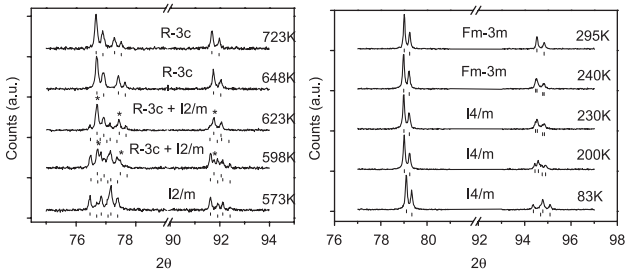

Evolution of structures as function of temperature in Ba_2SrWO_6 (left) and Ba_2CaWO_6 (right). The existence of two phase region in Ba_2SrWO_6 can be clearly seen by the progressive increase of the rhombohedral $R\bar{3}$ phase marked by asterisk (*).

Structure and magnetic properties of $Ca_2Fe_{1-x}Mn_xAlO_{5+\delta}$

M.D. Carvalho, L.P. Ferreira, J.C. Waerenborgh, E. Tsipis, A.B. Lopes and M. Godinho

Page 2530

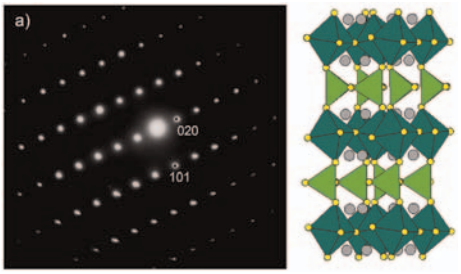

Structure of the $Ca_2Fe_{1-x}Mn_xAlO_5$ compound and electron diffraction pattern obtained along the [$\bar{1}$01] zone axis ($x = 0.2$), showing a brownmillerite structure.

Synthesis and characterization of a cadmium germanium phosphate $CdGe(OH)_3PO_4$ with an open framework

Yan Liu, Xiao-Li Yang, Gui-Li Wang, Jun Zhang, Yi-Zhi Li, Hong-Bin Du and Xiao-Zeng You

Page 2542

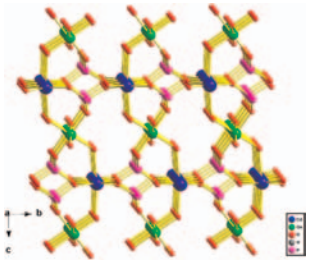

A new three-dimensional framework cadmium germanium phosphate, $CdGe(OH)_3PO_4$ was synthesized by solvothermal methods. The framework of $CdGe(OH)_3PO_4$ is built by a mixed network of GeO_6 octahedra, CdO_6 octahedra and PO_4 tetrahedra and contains a network of one-dimensional 3 and 6-membered ring channels. It belongs to a class of metal germanium phosphates with an open framework.

Erratum

Erratum to "Cerium effect on the phase structure, phase stability and redox properties of Ce-doped strontium ferrates" [J. Solid State Chem. 179 (2006) 3406–3419]

F. Deganello, L.F. Liotta, A. Longo, M.P. Casaletto and M. Scopelliti

Page 2547

Author inquiries

Submissions

For detailed instructions on the preparation of electronic artwork, consult the journal home page at http://authors.elsevier.com.

Other inquiries

Visit the journal home page (http://authors.elsevier.com) for the facility to track accepted articles and set up e-mail alerts to inform you of when an article's status has changed. The journal home page also provides detailed artwork guidelines, copyright information, frequently asked questions and more.

Contact details for questions arising after acceptance of an article, especially those relating to proofs, are provided after registration of an article for publication.

Language Polishing

Authors who require information about language editing and copyediting services pre- and post-submission should visit http://www.elsevier.com/wps/find/authorshome.authors/languagepolishing or contact authorsupport@elsevier.com for more information. Please note Elsevier neither endorses nor takes responsibility for any products, goods, or services offered by outside vendors through our services or in any advertising. For more information please refer to our Terms & Conditions at http://www.elsevier.com/wps/find/termsconditions.cws_home/termsconditions.

For a full and complete Guide for Authors, please refer to *J. Solid State Chem.,* Vol. 180, Issue 1, pp. *bmi–bmv*. The instructions can also be found at http://www.elsevier.com/wps/find/journaldescription.cws_home/622898/authorinstructions.

Journal of Solid State Chemistry has no page charges.